

Microfacet theory for non-uniform heightfields

EUGENE D'EON, NVIDIA, New Zealand

BENEDIKT BITTERLI, NVIDIA, USA

ANDREA WEIDLICH, NVIDIA, Canada

TIZIAN ZELTNER, NVIDIA, Switzerland

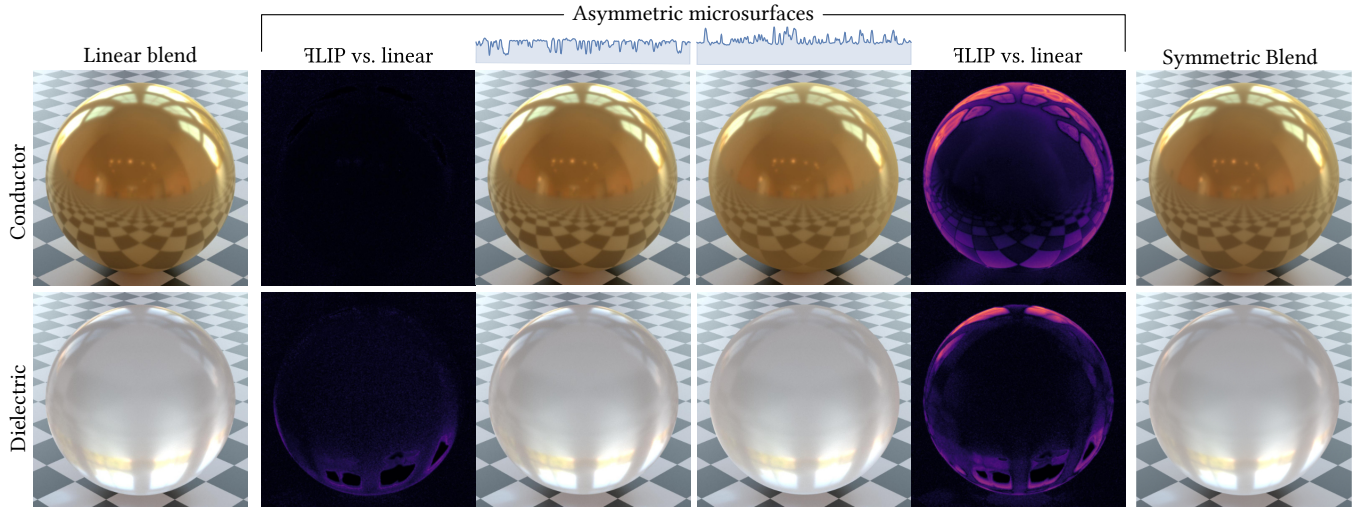


Fig. 1. Our asymmetric blending operator creates two new microfacet BSDFs (center) using the same blended NDF (GGX with roughness 0.02 and 0.8) but with different roughness applied to different elevation ranges of the microsurface (as seen in the top row profiles). The result is that while the interior of the surface remains unchanged, the silhouettes of the asymmetric BSDFs are different. At grazing angles, the spheres in the middle-right column appear rougher (note the reflection of the checkerboard onto the conductive spheres) because the rougher component of the mixture protrudes outward. This behavior cannot be achieved through a simple linear blend of two single-NDF BSDFs (as seen on the left).

We propose new methods for combining NDFs in microfacet theory, enabling a wider range of surface statistics. The new BSDFs that follow allow for independent adjustment of appearance at grazing angles, and can't be represented by linear blends of single-NDF BSDFs. We derive importance sampling for a symmetric operator that blends NDFs uniformly, and introduce a new asymmetric operator that supports NDF variation with elevation. We also extend Smith's model to support piecewise-constant NDF and material variations with elevation, and demonstrate accuracy via Monte Carlo simulations.

CCS Concepts: • Computing methodologies → Reflectance modeling.

Additional Key Words and Phrases: rough surface, BRDF, BSDF, Smith, asymmetric, eroded, damaged, NDF blend

ACM Reference Format:

Eugene d'Eon, Benedikt Bitterli, Andrea Weidlich, and Tizian Zeltner. 2023. Microfacet theory for non-uniform heightfields. In *Special Interest Group on Computer Graphics and Interactive Techniques Conference Conference Proceedings (SIGGRAPH '23 Conference Proceedings)*, August 6–10, 2023, Los Angeles, CA, USA. ACM, New York, NY, USA, 10 pages. <https://doi.org/10.1145/3588432.3591486>

SIGGRAPH '23 Conference Proceedings, August 6–10, 2023, Los Angeles, CA, USA
© 2023 Copyright held by the owner/author(s). Publication rights licensed to ACM.
This is the author's version of the work. It is posted here for your personal use. Not for redistribution. The definitive Version of Record was published in *Special Interest Group on Computer Graphics and Interactive Techniques Conference Conference Proceedings (SIGGRAPH '23 Conference Proceedings)*, August 6–10, 2023, Los Angeles, CA, USA, <https://doi.org/10.1145/3588432.3591486>.

Angeles, CA, USA. ACM, New York, NY, USA, 10 pages. <https://doi.org/10.1145/3588432.3591486>

1 INTRODUCTION

Microfacet bidirectional scattering distribution functions (BSDFs) are widely used in graphics as a primary tool for modeling the appearance of surfaces. Despite their accuracy, as demonstrated by comparisons to measured data [Tang and Buckius 1998] and Monte Carlo (MC) simulations [Heitz et al. 2016], the theory has limitations due to the assumptions of *geometrical optics*, *uniform statistics*, and *uniform material*. When these limitations prevent the theory from accurately modeling a surface, a common approach is to use a linear blend of multiple BSDFs with different properties. However, this approach does not represent all types of surfaces that we would like to simulate.

In this paper, we aim to extend the reach of microfacet theory by relaxing the assumptions of uniform statistics and uniform material in a rigorous way. We focus on these two assumptions, as the assumption of geometrical optics in microfacet theory and related alternative models have been addressed in other works [Holzschuch and Pacanowski 2017; Nayar et al. 1991; Tang et al. 1996].

The two uniformity assumptions of microfacet theory require that the normal distribution function (NDF), which describes how

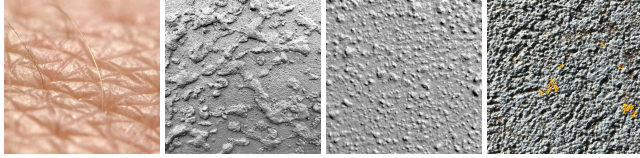


Fig. 2. Photographs of asymmetric surfaces (whose BSDF changes when the displacements are inverted), where the NDF is a function of elevation.

the surface deviates from a smooth plane, together with the material type (conductor, dielectric, or some other BSDF assigned to each microfacet) are both uniform over the microsurface—all elevation ranges must have the same material and normal statistics. These assumptions forbid the surface from having material variations that are correlated to elevation (such as white caps of an ocean surface). Also, the assumption of uniform statistics is incompatible with *asymmetric* heightfields, such as eroded, damaged, and pitted surfaces (Figure 2): for example, surfaces where the outward portion of the surface has a different roughness than the inward portion. When a surface exhibits a change of roughness with elevation, the outermost portion of the surface tends to dominate at grazing angles due to self occlusion (Figure 3). This leads to angle-dependent effects (Figure 4) that are not reproduced by a fixed linear combination of symmetric BSDFs (Figure 1).

To support a broader class of rough surface scattering, we extend Smith's microfacet model to support piecewise-uniform statistics and piecewise-uniform material, allowing for variation of both of these properties with elevation. We show how this allows for efficient evaluation and sampling of new microfacet BSDFs that exhibit angle-dependent blending of roughness and material properties. This allows new look development capabilities at the microsurface level. Authoring a surface using a linear blend of NDFs can now be performed in a variety of ways. In practice, this new flexibility allows for control over the silhouette of an object while leaving the rest unchanged (Figure 1). Linear mixtures of various roughnesses are typical in practice (for example for tissue [Graham et al. 2013]), and prior use of ad hoc view-dependent blending using Fresnel functions can now be avoided in favor of a physically-based approach.

A key insight of our work was to note that a wide range of interesting heightfields can be created from regular symmetric heightfields by applying different linear scalings to different elevation ranges (for example, scaling the negative displacements while leaving the positive values unchanged, as shown in Figure 5). To understand how these transformations manifest within microfacet theory, we take inspiration from the case of a *global* linear scaling of displacement: for shape-invariant NDFs, this simply results in a linear change in roughness [Heitz 2014]. This suggests that piecewise-linear stretching across various elevation ranges should create new heightfields of the same class but with elevation-dependent roughnesses. While this concept has no obvious interpretation in the original microfacet theory, it has a very direct interpretation in the more recent volumetric formulation of microfacet theory [Dupuy et al. 2016]. We leverage this correspondence to quantitatively evaluate our layered extension of Smith's theory by sampling realizations of explicit

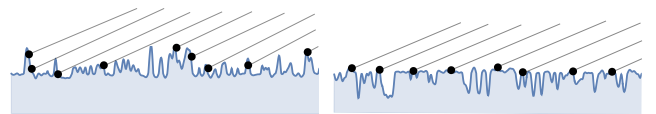


Fig. 3. Two asymmetric surfaces with the same NDF exhibit different appearance at grazing angles because the roughest component of the surface either occludes (left) or is occluded by (right) the less rough component.



Fig. 4. Close-up photograph of a glass bottle and a tomato at approximately normal incidence and grazing angle; both materials cannot be described with a single Beckmann or GGX distribution. Note that both objects exhibit a similar appearance at normal incidence, but for the bottle the highlight becomes broader at grazing angle whereas it becomes sharper on the tomato.

asymmetric surfaces and comparing MC simulations to our BSDFs, finding close agreement.

In summary, we present a new *asymmetric operator* for microfacet theory that permits elevation-varying normal and material properties, implemented as a *layered Smith volume* (Figure 5). Evaluation and sampling algorithms for these volumes are derived, and efficient application within a path tracer is demonstrated. For specular materials, the single-scattering portion of the BSDF can be solved in closed form. Stochastic evaluation is used for the multiple scattering component and for non-specular materials [Heitz et al. 2016]. For completeness, we also review and extend the *symmetric operator* that uniformly mixes two NDFs over the microsurface.

The rest of the paper is organized as follows. After reviewing prior work in the next section and prior microfacet theory in section 3 we outline our new theory in subsection 3.3. We describe our benchmark evaluation of the model in section 4. Results and implementation details for applying our model in a path tracer are given in section 5.

2 RELATED WORK

Our work builds on microfacet theory, which has a long history of modeling rough surfaces in graphics [Cook and Torrance 1982; Stam 2001; Walter et al. 2007]. Some early works considered generalizing the theory beyond the assumption of Gaussian (symmetric) statistics [Beckmann 1965, 1973], and several BRDFs for specific classes of asymmetric surfaces been presented [Koenderink et al. 1999]. We present a more general theory than these works, by supporting both non-uniform statistics and material. This is made possible by leveraging the more recent volumetric formulation of Smith's theory [Dupuy et al. 2016; Heitz 2014; Heitz et al. 2016; Smith 1967], which includes accurate bistatic visibility and multiple scattering.

Previous work has shown that using multiple NDFs is necessary to match a wide range of BSDF measurements. Instead of linearly mixing two BSDFs as a whole [Ngan et al. 2004] or decomposing the

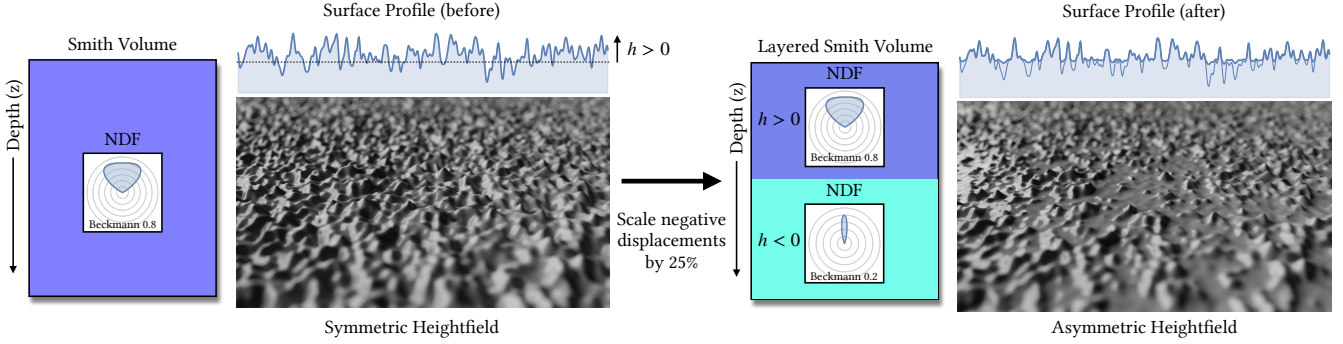


Fig. 5. A Beckmann heightfield with symmetric displacements $P(h)$ (left) is transformed into an asymmetric heightfield (right) by applying a piecewise-linear rescaling of the displacement values. We propose a layered volumetric representation of the transformed heightfield with a height-dependent NDF. This leads to a new scattering model that accurately predicts the reflectance from asymmetric surfaces and produces novel behaviours at grazing angles.

microfacet into two orthogonal piecewise representations [Bringier et al. 2020; Ribardière et al. 2019], we vary the statistical properties with elevation. This adds a new degree of freedom to express appearance and can be used to control grazing angles independently from normal incidence, which was previously only achieved by altering Fresnel reflectance [Barla et al. 2018] or other ad hoc blending methods.

Heitz and Neyret [2012] applied Smith’s theory for Beckmann surfaces to derive view-dependent filtering functions for color maps applied to Gaussian heightfields where the color varies with elevation. This was later [Heitz et al. 2013] extended to allow normal-correlated colors. Our work builds on these works by using similar equations to support specular materials, multiple scattering, and elevation-dependent roughness.

Our asymmetric operator is closely related to the Spongewake model [Wang et al. 2022] that approximates layered BSDFs using layered microflake volumes with two-sided flakes. This approach avoids the unwanted noise of Monte Carlo layer evaluations [Guo et al. 2018] or the precomputation and tabulation of numerical approaches [Jakob et al. 2014; Stam 2001; Zeltner and Jakob 2018]. Where Spongewake uses neural networks to predict multiple scattering, and other layered works use analytical approximations [Belcour 2018; Weidlich and Wilkie 2007], we use an unbiased random walk. For single-scattering, the fundamental difference of our approach is supporting one-sided microflakes that are required to describe heightfields.

3 THEORY

In this section we review previous microfacet theory, before deriving non-uniform generalizations in subsection 3.3. We express the scattering from a rough surface using a BSDF $f_s(\vec{\omega}_i, \vec{\omega}_o)$ [Pharr et al. 2016] in a coordinate frame where the geometric normal of the macro surface is $\vec{\omega}_g = (0, 0, 1)$. Following standard notation, both $\vec{\omega}_i$ and $\vec{\omega}_o$ point away from the surface. Current microfacet models overwhelmingly adopt Smith’s assumptions for a heightfield, which state that the NDF $D(\vec{\omega}_m)$ of microfacet orientations $\vec{\omega}_m$ is independent of elevation h . We will later (subsection 3.3) relax these

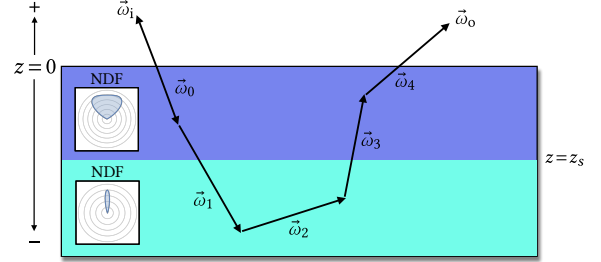


Fig. 6. An example four-collision path in a two-layer Smith volume where the NDF changes at depth z_s , illustrating our notation.

assumptions and extend Smith theory to elevation-correlated NDFs.

Under Smith’s assumption, the BSDF can be exactly described using a volumetric transport process (Figure 6) whereby a photon scatters within a volume governed by an asymmetric form of radiative transfer [Heitz et al. 2016]. Because all properties of the Smith volume are invariant to elevation h , it is possible to homogenize the medium to a half space ($z < 0$) with a uniform density [Dupuy et al. 2016]. This is simply a change of variable to use optical depth z , which simplifies the step PDFs and transmittances to exponentials. The mapping between microsurface elevation h and depth z in the homogenized volume follows from the probability density of elevations $P(h)$ with cumulative distribution function (CDF) $C(h)$ and inverse $C^{-1}(h)$ [Dupuy et al. 2016, (13),(14)],

$$z = \log(C(h)), \quad h = C^{-1}(\exp z). \quad (1)$$

In a homogenized Smith medium, the extinction coefficient $\sigma(\vec{\omega})$ and phase function $p(\vec{\omega} \rightarrow \vec{\omega}')$ are independent of optical depth z . In our notation, $\vec{\omega}$ and $\vec{\omega}'$ are the directions of motion before and after scattering respectively and we include absorption in the phase function (p is only normalized for lossless facets).

Given a Smith volume, the BSDF can be written as an integral over all possible paths inside the volume that begin at the surface of the half space ($z = 0$) in direction $\vec{\omega}_0 = -\vec{\omega}_i$ and undergo a sequence of collisions and scattering events until absorption or escape (Figure 6).

Without loss of generality, the extinction coefficient is unity when approaching the surface at normal incidence $\sigma(-\vec{\omega}_g) = 1$ and, more generally, $\sigma(\vec{\omega}) = (\vec{\omega} \cdot \vec{\omega}_g)\Lambda(\vec{\omega})$, where $\Lambda(\vec{\omega})$ is Smith's Lambda function [Heitz 2014; Walter et al. 2007].

3.1 Single Scattering

Single scattering represents an important special case for specular microfacets, as it can be derived in closed form. Here we briefly recall several results that we will reference later when generalizing the theory in the following section.

The single-scattering BRDF can be written as an expectation over collision depth z of transport along all two-segment paths in the homogenized half space [Dupuy et al. 2016]

$$\begin{aligned} f_1(\vec{\omega}_i, \vec{\omega}_o) &= \frac{p(-\vec{\omega}_i \rightarrow \vec{\omega}_o)}{\cos \theta_o} \int_{-\infty}^0 \frac{\sigma_i}{\cos \theta_i} \exp\left(\frac{z \sigma_i}{\cos \theta_i}\right) \exp\left(\frac{z \sigma_o}{\cos \theta_o}\right) dz \\ &= \frac{p(-\vec{\omega}_i \rightarrow \vec{\omega}_o)}{\cos \theta_o} \frac{\sigma_i / \cos \theta_i}{\sigma_i / \cos \theta_i + \sigma_o / \cos \theta_o}. \end{aligned} \quad (2)$$

Using $\sigma_j / \cos \theta_j = \Lambda(\vec{\omega}_j)$ and $\Lambda(-\vec{\omega}_j) = 1 + \Lambda(\vec{\omega}_j)$, the result simplifies to

$$f_1(\vec{\omega}_i, \vec{\omega}_o) = \frac{p(-\vec{\omega}_i \rightarrow \vec{\omega}_o)}{\cos \theta_o} \frac{\sigma_i}{\cos \theta_i} \frac{1}{1 + \Lambda(\vec{\omega}_i) + \Lambda(\vec{\omega}_o)} \quad (3)$$

$$= \frac{p(-\vec{\omega}_i \rightarrow \vec{\omega}_o)}{\cos \theta_o} \frac{\sigma_i}{\cos \theta_i} G_2(\vec{\omega}_i, \vec{\omega}_o) \quad (4)$$

to obtain the well-known bistatic Smith shadowing function G_2 [Heitz 2014]. Finally, expanding the phase function [Heitz et al. 2016, Eqs.(31,35)] produces the familiar form

$$f_1(\vec{\omega}_i, \vec{\omega}_o) = \frac{D(\vec{\omega}_m)F(\vec{\omega}_m)G_2(\vec{\omega}_i, \vec{\omega}_o)}{4 \cos \theta_i \cos \theta_o}. \quad (5)$$

3.2 Uniform Symmetric Blending of NDFs

In this section, we review the theory of symmetric NDF blending, which models microsurfaces with the same blended NDF at all elevations. Due to mutual self shadowing within the mixture, this theory produces BSDFs that deviate from a linear blend of two BSDFs (i.e. blended normal statistics \neq blended BSDF). This theory was first developed by Barla et al. [2018], and we extend it here with a new importance sampling method to allow its efficient use in a path tracer.

Specifically, we consider the BSDF of a heightfield whose NDF is a linear combination

$$D_{\text{mix}}(\vec{\omega}_m) = w_A D_A(\vec{\omega}_m) + w_B D_B(\vec{\omega}_m), \quad (6)$$

which is well-defined, so long as D_A and D_B are both valid heightfield NDFs and weights $w_A + w_B = 1$ are non-negative. Mixtures of three or more NDFs follow from recursively applying the present theory. By Smith's assumption, the blended normal statistics of D_{mix} are applied uniformly at all elevations, and therefore the surface must be *symmetric* (the BSDF is unchanged when the heightfield is inverted).

We now show that the single-scattering BSDFs and vNDF sampling for D_{mix} follow directly from those for D_A and D_B . Let $\Lambda_j(\vec{\omega})$ and $\sigma_j(\vec{\omega})$ be the Smith Lambda functions and extinction coefficients for D_j , where $j \in \{A, B\}$. Because a Smith extinction coefficient σ is

the normalization factor of the distribution of visible normals [Heitz et al. 2016], i.e.

$$\sigma(\vec{\omega}_i) = \int_{\Omega} \langle \vec{\omega}_i, \vec{\omega}_m \rangle D(\vec{\omega}_m) d\vec{\omega}_m, \quad (7)$$

and Λ is linearly related to σ , it follows that [Barla et al. 2018]

$$\Lambda_{\text{mix}}(\vec{\omega}) = w_A \Lambda_A(\vec{\omega}) + w_B \Lambda_B(\vec{\omega}) \quad (8)$$

$$\sigma_{\text{mix}}(\vec{\omega}) = w_A \sigma_A(\vec{\omega}) + w_B \sigma_B(\vec{\omega}). \quad (9)$$

The single-scattering BRDF (subsection 3.1) for the mixture depends on the heightfield properties only via Λ and D , and so it can be obtained by substituting Λ_{mix} and D_{mix} into Equation 4. Similarly, multiple scattering can be computed by using σ_{mix} to govern the random walk.

Importance Sampling. Importance sampling of the vNDF of the mixture can be done easily by decomposition, given sampling routines for the vNDFs of D_A and D_B . For photons colliding in the medium when moving in direction $\vec{\omega}$, the fraction that collide with a microfacet from component A is

$$P_A(\vec{\omega}) = \frac{w_A \sigma_A(\vec{\omega})}{\sigma_{\text{mix}}(\vec{\omega})} \quad (10)$$

due to the assumption of independent collisions in Equation 9. Sampling the vNDF of the mixture can therefore be performed by sampling from the vNDF of D_A with probability $P_A(\vec{\omega})$, and D_B otherwise (where, for a primary ray, $\vec{\omega} = -\vec{\omega}_i$).

Discussion. The key difference of symmetric NDF blending to a linear blend of BSDFs is due to the view-dependent occlusion of each NDF in the mixture. A direct consequence of Equation 10 is that the roughest component of the mixture eventually dominates at grazing angles. While this allows an alternative to blended BSDFs, there are many real and synthetic surfaces where the symmetry property does not hold (Figure 2) and a more general theory is required, which we give next.

3.3 Asymmetric Blending of NDFs

We now consider the asymmetric blending of two NDFs D_A and D_B . Our primary motivation is to model the scattering from a symmetric heightfield that has been deformed in a piecewise-linear fashion, as described in the introduction (Figure 5). In the volumetric formulation of microfacet theory, this results in different strata on the z axis with differing roughness, but of the same NDF class (assuming a shape invariant NDF). While this limited scope is the prime focus of our work (as it allows us to directly test our model), the new theory in this section supports completely independent NDF per strata (including distribution class and anisotropy).

We begin by showing that the NDF of a piecewise-homogeneous Smith half space is a linear combination of the NDFs D_j in the j th strata, $D_{\text{mix}} = \sum_j w_j D_j$. This follows from considering the statistics of visible normals as seen from straight down along $\vec{\omega}_g$. If NDF D_j is assigned to elevation range $[h_j, h_{j+1}]$, the blend weights are $w_j = \int_{h_j}^{h_{j+1}} P(h) dh$, and the corresponding strata boundaries (in terms of optical depth z) follow from Equation 1. This stratification offers an additional degree of freedom, beyond just the mixing weights, when forming a Smith volume that is a linear combination

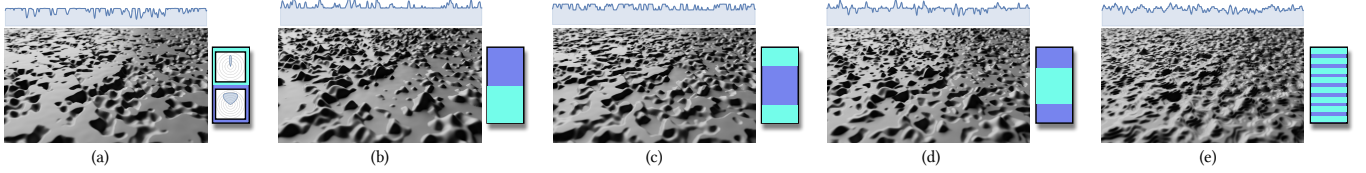


Fig. 7. Five microsurfaces with the same NDF: a 50/50 linear blend of Beckmann NDFs with roughnesses 1.0 and 0.02. Two distinct two-layer asymmetric surfaces (a,b) are represented in our model by layering the two NDFs in each of the two possible orders. Two symmetric variations are made using a symmetric layering 25%, 50%, 25% shown in (c,d). A fine alternate layering of the two roughness (e) approaches a surface with a uniform blended NDF at all heights. All five microsurfaces lead to distinct BSDFs.

of two NDFs; we give several examples in Figure 7. The resulting heightfields have significantly different reflectance behaviors than a uniform symmetric blend.

For simplicity, we will consider a two-stratum case for now where microfacets belonging to D_A occupy the top stratum. This is equivalent to a two-layer Smith medium (Figure 6) in which the medium properties follow D_A when $z \in [0, z_s]$ and D_B otherwise, where (using Equation 1)

$$z_s = \log(1 - w_A). \quad (11)$$

General layerings follow from recursively applying the two-layer theory to the bottom layer.

3.3.1 Multiple Scattering. We can simulate the full asymmetric BSDF using a random walk, much like for classical theory. Within each layer, the random walk behaves identically to the classical case, and we select the medium properties (phase function $\{p_A, p_B\}$ and extinction $\{\sigma_A, \sigma_B\}$) based on the z position of the walk. Care needs to be taken only when the random walk crosses over from one layer to the next, as free-flight distances sampled in one layer must be scaled appropriately when crossing over into the other layer. For reference, pseudocode is provided in the supplemental.

3.3.2 Single Scattering. To obtain a closed-form single-scattering BSDF for the asymmetric blend, we repeat the derivation from subsection 3.1 for our proposed layered Smith-medium. The single-scattering BSDF is

$$f_1(\vec{\omega}_i, \vec{\omega}_o) = f_{\text{top}}(\vec{\omega}_i, \vec{\omega}_o) + f_{\text{bot}}(\vec{\omega}_i, \vec{\omega}_o), \quad (12)$$

where f_{top} and f_{bot} are the scattered contributions from the top- and bottom layer respectively.

Top layer. The reflectance of the top layer can be derived analogously to the classical Smith volume reflectance, only with a finite medium extent (compare to Equation 2):

$$\begin{aligned} f_{\text{top}}(\vec{\omega}_i, \vec{\omega}_o) &= \frac{p_A(-\vec{\omega}_i \rightarrow \vec{\omega}_o)}{\cos \theta_o} \int_{z_s}^0 \frac{\sigma_{i,A}}{\cos \theta_i} \exp\left(\frac{z \sigma_{i,A}}{\cos \theta_i}\right) \exp\left(\frac{z \sigma_{o,A}}{\cos \theta_o}\right) dz \\ &= f_{1,A}(\vec{\omega}_i, \vec{\omega}_o) \left(1 - \exp\left(\frac{z_s \sigma_{i,A}}{\cos \theta_i} + \frac{z_s \sigma_{o,A}}{\cos \theta_o}\right)\right), \end{aligned} \quad (13)$$

where $f_{1,A}(\vec{\omega}_i, \vec{\omega}_o)$ is the single-scattering BSDF for a microsurface with NDF D_A .

Bottom layer. The bottom layer of the Smith volume is semi-infinite, and therefore acts identically to a classical Smith volume with NDF D_B (i.e. $f_{1,B}$). However, paths reaching the bottom layer

are attenuated by transmittance through the top layer along $\vec{\omega}_i$ and $\vec{\omega}_o$:

$$f_{\text{bot}}(\vec{\omega}_i, \vec{\omega}_o) = f_{1,B}(\vec{\omega}_i, \vec{\omega}_o) \exp\left(\frac{z_s \sigma_{i,A}}{\cos \theta_i} + \frac{z_s \sigma_{o,A}}{\cos \theta_o}\right). \quad (14)$$

Full single-scattering BSDF. Inserting Equation 13 and Equation 14 into Equation 12, we obtain

$$\begin{aligned} f_1(\vec{\omega}_i, \vec{\omega}_o) &= (1 - E(\vec{\omega}_i, \vec{\omega}_o)) f_{1,A}(\vec{\omega}_i, \vec{\omega}_o) + E(\vec{\omega}_i, \vec{\omega}_o) f_{1,B}(\vec{\omega}_i, \vec{\omega}_o) \\ \text{with } E(\vec{\omega}_i, \vec{\omega}_o) &= \exp\left(\frac{z_s \sigma_{i,A}}{\cos \theta_i} + \frac{z_s \sigma_{o,A}}{\cos \theta_o}\right). \end{aligned} \quad (15)$$

Remarkably, Equation 15 looks like a linear blend between BSDFs $f_{1,A}$ and $f_{1,B}$, but with an angle-dependent blending term $E(\vec{\omega}_i, \vec{\omega}_o)$. We can further relate this term to the bistatic shadowing function:

$$E(\vec{\omega}_i, \vec{\omega}_o) = \exp(z_s (\sigma_{i,A}/\cos \theta_i + \sigma_{o,A}/\cos \theta_o)) \quad (16)$$

$$= \exp(z_s (1 + \Lambda_A(\vec{\omega}_i) + \Lambda_A(\vec{\omega}_o))) \quad (17)$$

$$= \exp(z_s/G_{2,A}(\vec{\omega}_i, \vec{\omega}_o)). \quad (18)$$

This result differs from the BRDF derivation in Spongewake [Wang et al. 2022] by accounting for the asymmetric coefficients $\sigma(\vec{\omega}) \neq \sigma(-\vec{\omega})$ of the one-sided flakes (and differs by the appearance of a 1 in the denominator of G_2).

For a two-layer volume with NDF given by Equation 6 we have (using the optical depth mapping in Equation 11)

$$E(\vec{\omega}_i, \vec{\omega}_o) = (1 - w_A)^{1/G_{2,A}(\vec{\omega}_i, \vec{\omega}_o)} = (w_B)^{1/G_{2,A}(\vec{\omega}_i, \vec{\omega}_o)}. \quad (19)$$

The angular-dependence of Equation 19 clearly demonstrates how a two-layer model differs from a linear blend of BSDFs. The latter corresponds to E being a constant, which is only possible when $G_{2,A}$ is a constant. This can only occur if the top layer has zero roughness, to prevent interreflection between the two layers. This is the unique case in which a linear blend of two microfacet BRDFs has an exact correspondence within the layered Smith theory. Interestingly, this case requires that the rough component of the mixture induces a purely negative (inward) displacement (similar to Figure 7 (a)).

Importance Sampling. Following Wang et al. [2022], we importance sample f_1 in Equation 15 by sampling directions from the vNDF of either D_A or D_B , with probability P_A and $P_B = 1 - P_A$ respectively. We set P_A to be the probability that a ray entering the Smith volume from $-\vec{\omega}_i$ will collide in the top layer, i.e. $P_A = 1 - \exp(z_s \sigma_i)$.

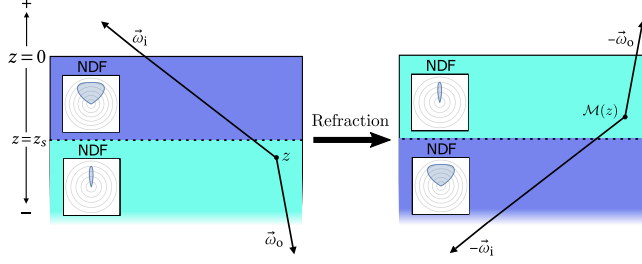


Fig. 8. Refracting through a microfacet (here at depth z in the bottom layer) “flips” the Smith volume upside-down, such that directions are negated, the layers are switched, and positions in the refracting layer are remapped through the mapping $\mathcal{M}(z) = \log(1 - \exp(z))$. All interactions with the Smith volume after refraction occur in the flipped configuration.

3.3.3 Dielectric Microfacets. So far, our derivations focused on purely reflecting microfacets, and extra care needs to be taken to handle refraction. In a Smith volume, a refraction event “flips” the Smith volume upside down, such that directions after refraction are negated and the z coordinate is transformed through a mapping $\mathcal{M}(z)$ (Figure 8). This requires a separate derivation of the single-scattering BSDF for dielectrics.

For now, we will focus on the expected probability of traversing through a layered Smith volume if a refraction event occurs in the bottom layer. Without loss of generality, we assume $\cos \theta_i > 0$ and $\cos \theta_o < 0$. The ray traverses the top layer (incurring a transmittance), collides in the bottom layer, refracts, and exits the bottom layer (incurring another transmittance) from a “flipped” configuration, where media properties are evaluated with negated direction $-\vec{\omega}_o$ and remapped coordinate $\mathcal{M}(z) = \log(1 - \exp(z))$ [Dupuy et al. 2016]. With attenuation $T_A = \exp(z_s \Lambda_A(-\vec{\omega}_i))$ in the top layer, the expected exit probability is then (c.f. Equation 2):

$$\begin{aligned} P_{\text{bot}} &= T_A \int_{-\infty}^{z_s} \exp\left(\frac{(z - z_s) \sigma_B(-\vec{\omega}_i)}{\cos \theta_i}\right) \exp\left(\frac{\mathcal{M}(z) \sigma_B(-\vec{\omega}_o)}{|\cos \theta_o|}\right) dz \\ &= B(w_B; \Lambda_B(\vec{\omega}_i) + 1, \Lambda_B(-\vec{\omega}_o) + 1) \cdot (w_B)^{\Lambda_A(\vec{\omega}_i) - \Lambda_B(\vec{\omega}_i)}, \end{aligned} \quad (20)$$

where $B(w_B; a, b)$ is the incomplete Beta function (see supplemental). Similarly, if refraction occurs in the top layer, we obtain

$$P_{\text{top}} = B(w_A; \Lambda_A(-\vec{\omega}_o) + 1, \Lambda_A(\vec{\omega}_i) + 1) \cdot (w_A)^{\Lambda_B(-\vec{\omega}_o) - \Lambda_A(-\vec{\omega}_o)}.$$

These traversal probabilities are in fact the equivalent of the bistatic Smith shadowing function G_2 for refraction in a layered Smith volume. We can verify that if the medium properties of the top and bottom layers are the same, we have $P_{\text{bot}} + P_{\text{top}} = B(\sigma_i, \sigma_o)$, which is the well-known bistatic shadowing function for classical dielectric microfacets [Heitz et al. 2016; Pinel et al. 2005].

With the bistatic shadowing function in hand, we can now write the single-scattering BSDF for refraction (c.f. Equation 4):

$$f_{1,\text{refract}}(\vec{\omega}_i, \vec{\omega}_o) = \frac{p_A(-\vec{\omega}_i \rightarrow \vec{\omega}_o) \sigma_{i,A} P_{\text{top}} + p_B(-\vec{\omega}_i \rightarrow \vec{\omega}_o) \sigma_{i,B} P_{\text{bot}}}{|\cos \theta_o \cos \theta_i|} \quad (21)$$

For dielectric microfacets, phase function p_A is [Heitz et al. 2016]

$$p_{A,\text{refract}}(-\vec{\omega}_i \rightarrow \vec{\omega}_o) = \frac{\langle \vec{\omega}_i, \vec{\omega}_m \rangle \langle \vec{\omega}_o, \vec{\omega}_m \rangle (1 - F(\vec{\omega}_i, \vec{\omega}_m)) D_A(\vec{\omega}_m)}{(\eta \langle \vec{\omega}_i, \vec{\omega}_m \rangle + \langle \vec{\omega}_o, \vec{\omega}_m \rangle)^2 \sigma_A(-\vec{\omega}_i)},$$

and similarly for p_B . Here, η is the relative index of refraction, $\vec{\omega}_m$ is the half-vector for refraction [Walter et al. 2007] and F is the Fresnel term. Inserting the above into Equation 21 then gives the complete single-scattering BSDF for refraction. The single-scattering BSDF for reflection from dielectrics is identical to Equation 15.

3.3.4 Non-Uniform Material. It’s possible to assign differing material properties to each layer in the Smith volume. For specular materials, we apply independent Fresnel terms to each component of the expanded single-scattering BSDF (Equation 15). For multiple scattering and non-specular materials, the microfacet BSDF is varied with elevation during NEE and phase function sampling.

4 VALIDATION

To validate our model, we generated square tileable realizations of Beckmann heightfields using Fourier transforms (see also [Heitz 2015]), transformed them using piecewise-linear stretching and computed reference BSDF solutions using ray tracing. For each benchmark configuration we varied the incident angle θ_i over a range of values and accumulated histograms of $f_s(\vec{\omega}_i, \vec{\omega}_o) \cos \theta_o$ into 2D images, separating the first three orders of scattering into individual tallies. We verified that our symmetric Beckmann heightfields and benchmark simulations closely match the BSDF of previous work [Heitz et al. 2016].

To quantify the accuracy of our layered-Smith model for asymmetric heightfields, we ran a number of $w_A = w_B = 0.5$ two-layer benchmarks with the low and high roughnesses in both top and bottom configurations and compared to predictions of our model and to a linear blend of BSDFs. Figure 13 shows benchmark results for a rough mirror with roughnesses 0.91 and 0.364 for two illumination angles. Figure 13 (a) shows a typical example seen throughout our benchmark suite: for moderate inclinations, all three BSDFs are similar over all scattering orders. However, as the illumination is tilted to near grazing (b) we see the failure of the linear blend to occlude the sharp reflection due the outwardly protruding rougher component of the mixture. Our layered BSDFs properly model the mutual occlusion of the NDFs. We observed a continuation of these trends for diffuse and dielectric facets (see supplemental), and observed a consistent match between BSDF and benchmark with an accuracy that is comparable to prior comparisons using uniform heightfields. From these results, we conclude that a layered extension of Smith volumes produces BSDFs that accurately model (under the assumption of geometrical optics) multiple scattering from a well-defined and plausible class of asymmetric surfaces.

5 RESULTS

Implementation details. We implemented our reflectance model in the Mitsuba Renderer [Jakob 2010] for two-layer asymmetric mixtures with either diffuse, dielectric or conductor facets. We included support for independent diffuse color and conductor properties in each layer. We found the performance of the two-layer model to be about 20% slower render time than a single-NDF BSDF with multiple scattering and comparable to the cost of a linear blend of BSDFs. Our theory supports general NDFs in the layering, but in practice a sampling procedure for the visible distribution of normals (vNDF) [Heitz and d’Eon 2014] is required for efficient path

tracing. Therefore, we limit our results to Beckmann [Blinn 1977] and Trowbridge-Reitz/GGX[Walter et al. 2007].

The differences between the various BSDFs can be subtle and we ask the reader to view the supplemental material where image sequences can be flipped between to better highlight the differences. We further include TLIP image comparisons [Andersson et al. 2020] throughout this section to highlight the perceived differences.

We found naive unidirectional evaluation of the stochastic BSDFs to produce excessively high variance for configurations with $\alpha_{\text{top}} > \alpha_{\text{bot}}$. We therefore evaluate the random walks in a bidirectional manner, as discussed by Heitz et al. [2016]. An example of the variance reduction is provided in the supplemental material.

Rough Conductors. Figure 10 shows a two-layer rough conductor where roughness of 0.8 on the lower layer is used to create inward damage to the smooth 0.01 base surface. The damage is varied between renders by changing the two-layer mixing parameter w_A .

In our experiments we found the case of $\alpha_{\text{top}} < \alpha_{\text{bot}}$ to be visually very similar to a linear blend of the two BRDFs, suggesting that a linear blend of BRDFs approximates an *asymmetric* surface. However, provided $\alpha_{\text{top}} > 0$, there is always a grazing angle where the two differ. This can be seen in Figure 12 where we compare two-layer rough gold surfaces to a linear blend. In this scene a very wide field of view and extended geometry show a wide range of incident angles in the same image. Near the light source the viewing angle is very near grazing and a distinct difference is visible very near the light source across the three BSDFs. The same differences remain visible in more natural scenes, e.g. involving environment illumination or more complex geometry in Figure 1 (a) and Figure 14 (a) respectively.

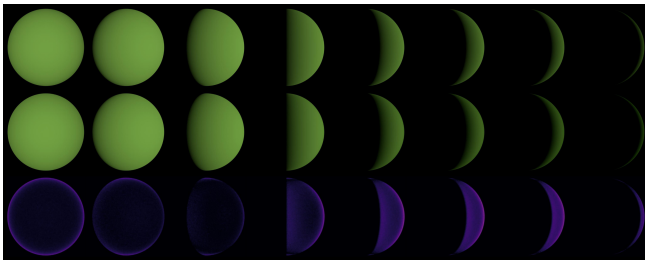


Fig. 9. Asymmetric rough diffuse BRDF comparison: $w_A = 0.5$ blend of Trowbridge-Reitz roughness 0.2 and 0.8 with Lambertian facets (albedo {0.3, 0.6, 0.1}) where the light position is moved from left to right in each row with the BRDF held constant. **Top row:** $\alpha_{\text{top}} < \alpha_{\text{bot}}$. **Middle row:** $\alpha_{\text{top}} > \alpha_{\text{bot}}$. **Bottom row:** TLIP difference between the two.

Rough Diffuse. In Figure 9 and Figure 11 (a) we compare asymmetric rough diffuse BRDFs under directional and environment illumination respectively. The difference in the microsurface profiles results in a slight variation in behaviour for grazing lighting and at the silhouette, consistent with the findings in our benchmarks.

Rough Dielectrics. The discussion of appearance differences between two-layer microsurfaces with dielectric facets (as shown in Figure 11 (c) and Figure 14 (b)) is slightly more nuanced. While we still observe clear intensity changes in reflected light at grazing

angles, this effect is much weaker for aspects of the appearance dominated by transmission. This is expected as light scattering through a dielectric object must necessarily also interact with a flipped version of the asymmetric heightfield when leaving the material and therefore the ordering of roughnesses on the top or bottom becomes less relevant. Interestingly, transmitted light in both configurations ($\alpha_{\text{top}} < \alpha_{\text{bot}}$ and $\alpha_{\text{top}} > \alpha_{\text{bot}}$) scatters quite differently compared to a linear blend of both roughnesses while the former case tends to be visually very close to the linear blend for other material types.

Our asymmetric microsurfaces can also be used to construct a dielectric coating that is applied on top of other BSDFs, e.g. on top of a Lambertian material (Figure 11 (d)). Here, two nested random walks are required to evaluate all multiple scattering that occurs inside the heightfield and between the two BSDF layers [Guo et al. 2018]. The observed appearance differences of the asymmetric model in this setting are similar to the reflective component in Figure 11 (c).

Edge color variation. We are also free to vary material properties apart from the NDF roughness in each layer of the Smith volume. It is straightforward to include this in an implementation by, e.g., changing the complex index of refraction of conductor facets or the albedo of diffuse facets during the local phase function evaluation at each interaction of the random walk. This approach allows for even greater control of reflected color and intensity at grazing angles as we illustrate in Figures 16, 17, and 15.

6 CONCLUSION

In this paper we have presented a new reflectance model for rough surfaces that efficiently and accurately simulates multiple scattering from heightfields with height-dependent roughness and material properties, such as damaged and eroded surfaces. We based our model on a layered-Smith microfacet theory that subsumes prior Smith BSDFs as a special case and provides a new physically-based approach for blending NDFs that allows flexible control of the grazing behaviour. We established a new correspondence between deformed heightfields and piecewise-homogeneous Smith volumes and used this to produce benchmarks that validated our model’s numerical accuracy while simultaneously illuminating the limitations of a linear blend of BSDFs.

Limitations. Future work is required to determine if our new BSDFs serve as a practical tool for fitting real-world measurements. A thorough comparison or a related study examining surface profiles with height-varying NDFs would be required to ascertain whether a piecewise constant NDF sufficiently characterizes asymmetric surfaces or if introducing continuous variation of NDF would yield substantially different results from our current model. Moving beyond piecewise-constant variation of NDF and material would greatly complicate distance sampling, shadowing/masking and likely lead to non-tractable single-scattering components.

ACKNOWLEDGMENTS

We thank Reviewer 1 for noting that the symmetric blend of two NDFs was considered previously. We also thank Eric Heitz for helpful technical discussions, Matt Pharr for proofreading, and Ignacio Llamas and Aaron Lefohn for supporting this research.

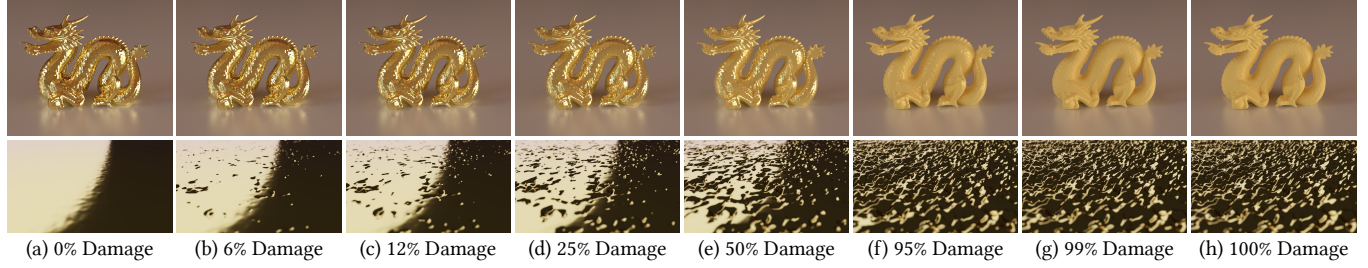


Fig. 10. Modeling inward damage of a gold microsurface using a two-layer configuration with roughnesses 0.01 and 0.8. Below each dragon render we show a render of an example microsurface that is consistent with the BSDF used on the image above. The moderately damaged renders (b-d) maintain the appearance of shiny gold while filling in the darker reflections and avoiding an adverse roughening of the silhouette.

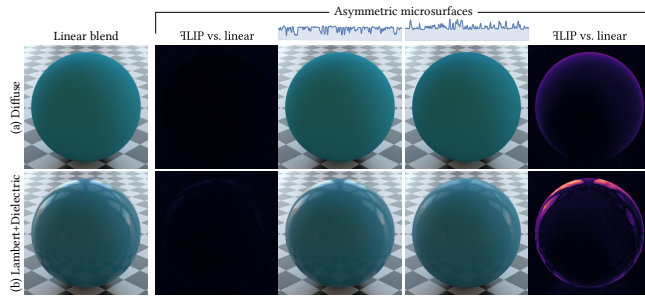


Fig. 11. Comparison of $w_A = 0.5$ dual Trowbridge-Reitz NDFs against a linear blend. (a) Diffuse facets with albedo $\{0.05, 0.6, 0.8\}$. (b) Rough dielectric coating on top of a Lambertian base. All configurations use an equal mix of roughnesses 0.02 and 0.8 and are lit by the same environment illumination. See the supplemental material for an analogous comparison using Beckmann NDFs.

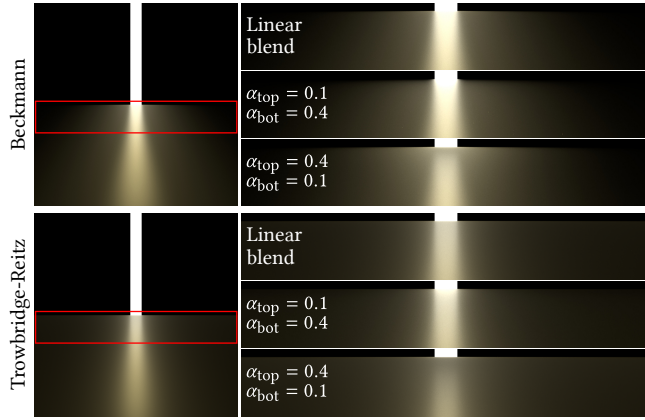
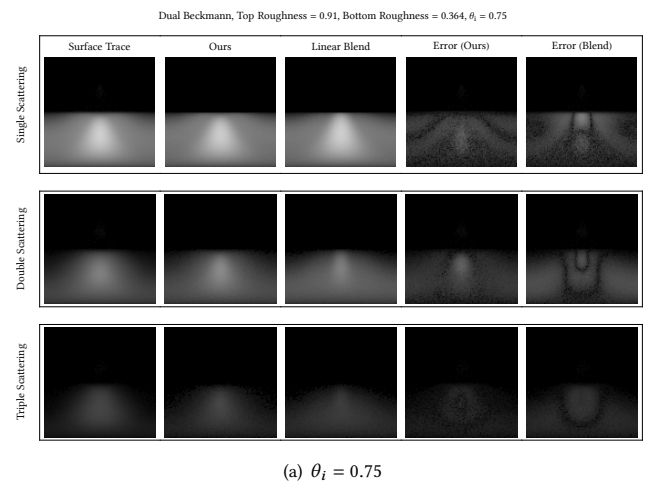
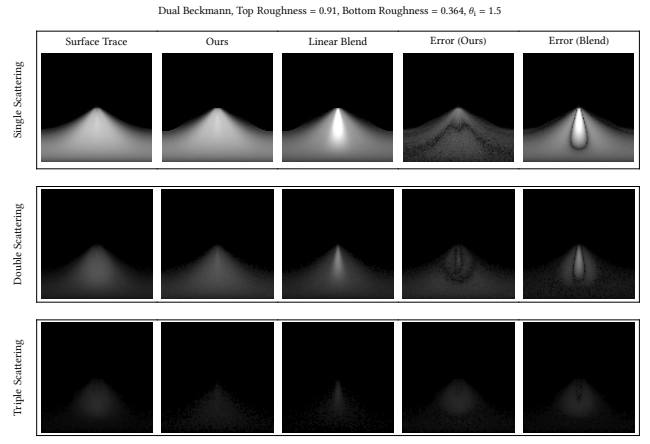


Fig. 12. A white strip light reflecting off a rough gold surface. For both NDF types we see (near the light source) a distinct difference between our layered models and a linearly blended BRDF.



(a) $\theta_i = 0.75$



(b) $\theta_i = 1.5$

Fig. 13. Two-layer Beckmann rough conductor benchmark for two illumination angles. We see a close agreement between our model and the ground truth surface trace for the first three orders of scattering. The linear blend is a close approximation to our model except at grazing angles (b) where the larger roughness in the top layer completely occludes the smaller roughness. The left three images in each configuration display $f_s \cos \theta$ with a gamma correction of 0.3. The error images display a difference in linear space, followed by a gamma correction of 0.3.

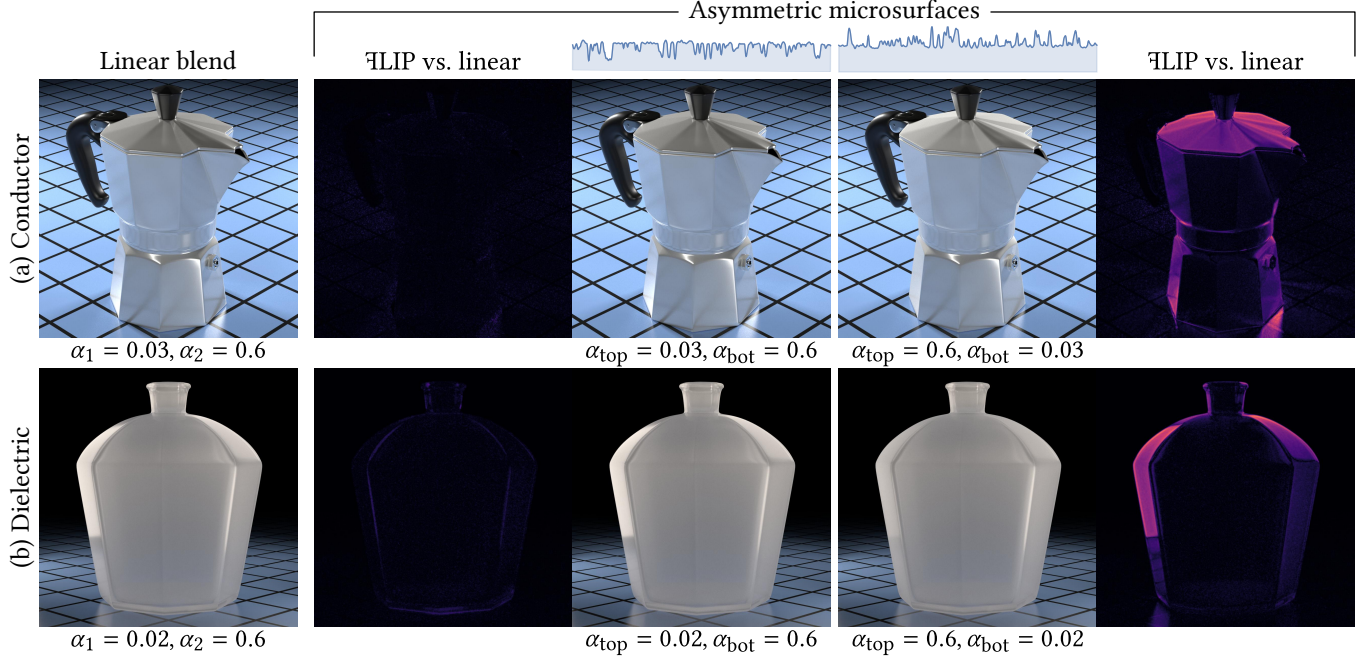


Fig. 14. Dual ($w_A = 0.5$) Trowbridge-Reitz NDFs applied to more complex geometry under smooth studio lighting. In both the conductor (a) and dielectric (b) setting, the asymmetric microsurfaces enable fine control over the reflective properties at grazing angles which cannot be achieved by a simple linear blend.

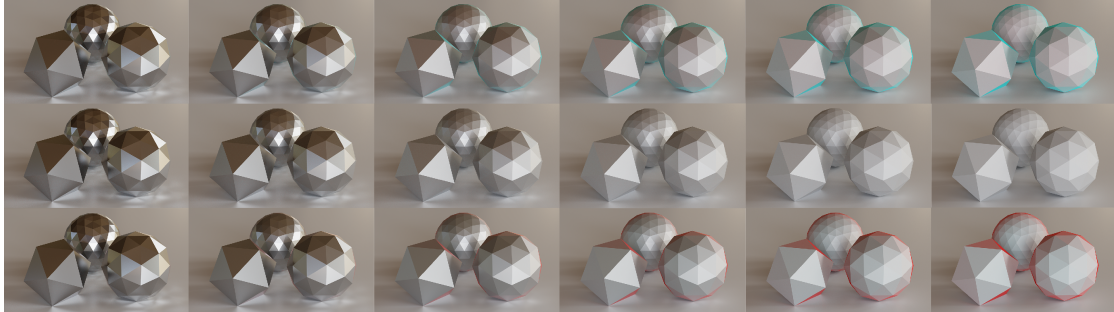


Fig. 15. Uniform GGX conductors with roughnesses 0.05, 0.1, 0.2, 0.3, 0.4, 0.5 (left to right) and equal blend of two conductor colors (top row: cyan on top, middle: linear blend, bottom row: red on top). Note how the topmost color dominates at grazing for high roughness (right).

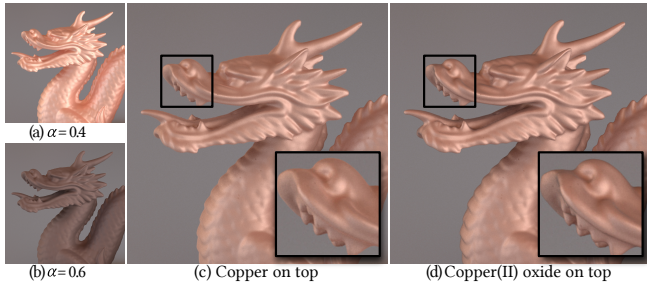


Fig. 16. Two Trowbridge-Reitz NDFs with conductor facets of different materials and roughnesses (a) & (b) are combined into asymmetric microsurfaces with $w_A = 0.5$. We observe subtle color differences at grazing angles depending on the order of the two layers (c) & (d).

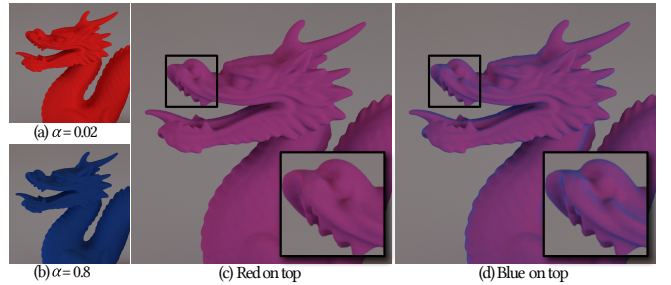


Fig. 17. Two Trowbridge-Reitz NDFs with diffuse facets (a) & (b) are combined into asymmetric microsurfaces with $w_A = 0.5$. $\alpha_{\text{top}} < \alpha_{\text{bot}}$ (c) looks like we expect from a linear blend whereas $\alpha_{\text{top}} > \alpha_{\text{bot}}$ (d) causes color variation at grazing angles due to the shadowed lower layer.

REFERENCES

- Pontus Andersson, Jim Nilsson, Tomas Akenine-Möller, Magnus Oskarsson, Kalle Åström, and Mark D. Fairchild. 2020. 3LIP: A Difference Evaluator for Alternating Images. *Proceedings of the ACM on Computer Graphics and Interactive Techniques* 3, 2 (2020), 15:1–15:23. <https://doi.org/10.1145/3406183>
- Pascal Barla, Romain Pacanowski, and Peter Vangorp. 2018. A Composite BRDF Model for Hazy Gloss. *Computer Graphics Forum* 37, 4 (07 2018), 55–66. <https://doi.org/10.1111/cgf.13475>
- Petr Beckmann. 1965. Scattering by composite rough surfaces. *Proc. IEEE* 53, 8 (1965), 1012–1015. <https://doi.org/10.1109/PROC.1965.4081>
- Petr Beckmann. 1973. Scattering by non-Gaussian surfaces. *IEEE Transactions on Antennas and Propagation* 21, 2 (1973), 169–175. <https://doi.org/10.1109/TAP.1973.1140444>
- Laurent Belcour. 2018. Efficient Rendering of Layered Materials using an Atomic Decomposition with Statistical Operators. *ACM Transactions on Graphics (TOG)* 37, 4 (2018). <https://doi.org/10.1145/3197517.3201289>
- James F. Blinn. 1977. Models of light reflection for computer synthesized pictures. *Proceedings of 4th annual conference on Computer graphics and interactive techniques* (1977), 192–198. <https://doi.org/10.1145/563858.563893>
- Benjamin Bringier, Mickaël Ribardière, Daniel Meneveaux, and Lionel Simonot. 2020. Design of rough microgeometries for numerical simulation of material appearance. *Appl. Opt.* 59, 16 (Jun 2020), 4856–4864. <https://doi.org/10.1364/AO.391254>
- Robert L. Cook and K.E. Torrance. 1982. A reflectance model for computer graphics. In *ACM Trans. Graphic.*, 7–24. <https://doi.org/10.1145/357290.357293>
- Jonathan Dupuy, Eric Heitz, and Eugene d'Eon. 2016. Additional Progress Towards the Unification of Microfacet and Microflake Theories.. In *EGSR (EI&I)*, 55–63. <http://dx.doi.org/10.2312/sre.20161210>
- Paul Graham, Borom Tunwattanapong, Jay Busch, Xueming Yu, Andrew Jones, Paul Debevec, and Abhijeet Ghosh. 2013. Measurement-based synthesis of facial microgeometry. In *Computer Graphics Forum*, Vol. 32. Wiley Online Library, 335–344. <https://doi.org/10.1111/cgf.12053>
- Yu Guo, Miloš Hašan, and Shuang Zhao. 2018. Position-free Monte Carlo simulation for arbitrary layered BSDFs. *ACM Transactions on Graphics (TOG)* 37, 6 (2018), 1–14. <https://doi.org/10.1145/3272127.3275053>
- Eric Heitz. 2014. Understanding the masking-shadowing function in microfacet-based BRDFs. *Journal of Computer Graphics Techniques* 3, 2 (2014), 32–91. <http://jcgta.org/published/0003/02/03/>
- Eric Heitz. 2015. *Generating Procedural Beckmann Surfaces*. Technical Report. <https://eheitzresearch.wordpress.com/research/>
- Eric Heitz and Eugene d'Eon. 2014. Importance sampling microfacet-based BSDFs using the distribution of visible normals. In *Computer Graphics Forum*, Vol. 33. Wiley Online Library, 103–112. <https://doi.org/10.1111/cgf.12417>
- Eric Heitz, Johannes Hanika, Eugene d'Eon, and Carsten Dachsbacher. 2016. Multiple-scattering microfacet BSDFs with the Smith model. *ACM Transactions on Graphics (TOG)* 35, 4 (2016), 58. <https://doi.org/10.1145/2897824.2925943>
- Eric Heitz and Fabrice Neyret. 2012. Representing appearance and pre-filtering subpixel data in sparse voxel octrees. In *EGGH-HPG'12-Eurographics conference on High Performance Graphics*. Eurographics, 125–134. <https://hal.inria.fr/hal-00704461/>
- Eric Heitz, Derek Nowrouzezahrai, Pierre Poulin, and Fabrice Neyret. 2013. Filtering color mapped textures and surfaces. In *Proceedings of the ACM SIGGRAPH Symposium on Interactive 3D Graphics and Games*. 129–136.
- Nicolas Holzschuch and Romain Pacanowski. 2017. A two-scale microfacet reflectance model combining reflection and diffraction. *ACM Transactions on Graphics (TOG)* 36, 4 (2017), 1–12. <https://doi.org/10.1145/3072959.3073621>
- Wenzel Jakob. 2010. Mitsuba renderer. <http://www.mitsuba-renderer.org>.
- Wenzel Jakob, Eugene d'Eon, Otto Jakob, and Steve Marschner. 2014. A comprehensive framework for rendering layered materials. *ACM Transactions on Graphics (ToG)* 33, 4 (2014), 1–14. <https://doi.org/10.1145/2601097.2601139>
- Jan J Koenderink, Andrea J Van Doorn, Kristin J Dana, and Shree Nayar. 1999. Bidirectional reflection distribution function of thoroughly pitted surfaces. *International Journal of Computer Vision* 31, 2-3 (1999), 129–144. <https://doi.org/10.1023/A:1008061730969>
- S.K. Nayar, K. Ikeuchi, and T. Kanade. 1991. Surface reflection: physical and geometrical perspectives. *IEEE Transactions on Pattern Analysis and Machine Intelligence* 13, 7 (1991), 611–634. <https://doi.org/10.1109/34.85654>
- Addy Ngan, Frédéric Durand, and Wojciech Matusik. 2004. Experimental Validation of Analytical BRDF Models. In *ACM SIGGRAPH 2004 Sketches* (Los Angeles, California) (*SIGGRAPH '04*). Association for Computing Machinery, New York, NY, USA, 90. <https://doi.org/10.1145/1186223.1186336>
- Matt Pharr, Wenzel Jakob, and Greg Humphreys. 2016. *Physically based rendering: From theory to implementation*. Morgan Kaufmann.
- Nicolas Pinel, Christophe Bourlier, and Joseph Saillard. 2005. Energy conservation of the scattering from one-dimensional random rough surfaces in the high-frequency limit. *Optics Letters* 30, 15 (2005), 2007–2009. <https://doi.org/10.1364/OL.30.002007>
- Mickaël Ribardière, Benjamin Bringier, Lionel Simonot, and Daniel Meneveaux. 2019. Microfacet BSDFs Generated from NDFs and Explicit Microgeometry. *ACM Trans. Graph.* 38, 5, Article 143 (jun 2019), 15 pages. <https://doi.org/10.1145/3338697>
- Bruce Smith. 1967. Geometrical shadowing of a random rough surface. *IEEE transactions on antennas and propagation* 15, 5 (1967), 668–671. <https://doi.org/10.1109/TAP.1967.1138991>
- Jos Stam. 2001. An Illumination Model for a Skin Layer Bounded by Rough Surfaces. In *Rendering Techniques*. 39–52. https://doi.org/10.1007/978-3-7091-6242-2_4
- Kakuen Tang and Richard O Buckius. 1998. The geometric optics approximation for reflection from two-dimensional random rough surfaces. *International Journal of Heat and Mass Transfer* 41, 13 (1998), 2037–2047. [https://doi.org/10.1016/S0017-9310\(97\)00227-5](https://doi.org/10.1016/S0017-9310(97)00227-5)
- Kakuen Tang, Ralph A Dimenna, and Richard O Buckius. 1996. Regions of validity of the geometric optics approximation for angular scattering from very rough surfaces. *International Journal of Heat and Mass Transfer* 40, 1 (1996), 49–59. [https://doi.org/10.1016/S0017-9310\(96\)00073-7](https://doi.org/10.1016/S0017-9310(96)00073-7)
- B. Walter, S.R. Marschner, H. Li, and K.E. Torrance. 2007. Microfacet models for refraction through rough surfaces. In *Rendering Techniques (Proc. EG Symposium on Rendering)*. Citeseer, 195–206. <http://dx.doi.org/10.2312/EGWR/EGSR07/195-206>
- Beibei Wang, Wenhua Jin, Miloš Hašan, and Ling-Qi Yan. 2022. SpongeCake: A Layered Microflake Surface Appearance Model. *ACM Transactions on Graphics (TOG)* 42, 1 (2022), 1–16. <https://doi.org/10.1145/3546940>
- Andrea Weidlich and Alexander Wilkie. 2007. Arbitrarily layered micro-facet surfaces. In *Proceedings of the 5th international conference on Computer graphics and interactive techniques in Australia and Southeast Asia*. 171–178.
- Tizian Zeltner and Wenzel Jakob. 2018. The layer laboratory: a calculus for additive and subtractive composition of anisotropic surface reflectance. *ACM Transactions on Graphics (TOG)* 37, 4 (2018), 1–14. <https://doi.org/10.1145/3197517.3201321>